Journal of Solution Chemistry (2020) 49:885–901
https://doi.org/10.1007/s10953-020-00978-0

Solid–Liquid Phase Equilibria in the Quinary System Na^+, K^+, Mg^{2+}//Cl^-, NO_3^-–H_2O and Its Subsystems at 258 K

Xue-Ying Wang[1] · Xue-Li Huang[1,2] · Xue-Feng Wang[1,2] · Ze-Yan Sun[1] · Qing-Long Luo[1] · He Huang[1]

Received: 29 September 2019 / Accepted: 27 January 2020 / Published online: 2 August 2020

Abstract
The phase equilibrium of the quaternary system Na^+, K^+, Mg^{2+}//Cl^-–H_2O and the quinary system Na^+, K^+, Mg^{2+}//Cl^-, NO_3^-–H_2O were investigated at 258 K using the isothermal dissolution equilibrium method. The phase diagrams were obtained based on the measured data. Double salt $KCl{\cdot}MgCl_2{\cdot}6H_2O$ was found in the quaternary and the quinary systems at 258 K. In the quaternary system Na^+, K^+, Mg^{2+}//Cl^-–H_2O, there are two invariant points, five univariant curves, and four crystallization fields. The quinary system saturated with $NaCl{\cdot}2H_2O$ contains four invariant points, nine univariant curves, and six crystallization fields corresponding to KCl, $NaNO_3$, KNO_3, $Mg(NO_3)_2{\cdot}6H_2O$, $KCl{\cdot}MgCl_2{\cdot}6H_2O$ and $MgCl_2{\cdot}8H_2O$. $Mg(NO_3)_2{\cdot}6H_2O$ and $MgCl_2{\cdot}8H_2O$ that have higher concentrations and stronger salting-out effect on other salts. Therefore, low-temperature pretreatment can offer an alternative treatment of brines in accordance with the necessity for current brine treatment processes to reduce the presence of double salts and be crucial for purer products to be separated.

Keywords Nitrate · Low temperature · Double salt · Solubility

1 Introduction

Nitrate brines are found in the area close to Lop Nur in Xinjiang Province of China, containing Na^+, K^+, Mg^{2+}, Cl^-, NO_3^-, SO_4^{2-}, which can be used to produce potassium nitrate or sodium nitrate, and play important roles in many industrial fields [1, 2]. However, the brine treatment process is difficult because the separation processes are extremely complex at normal temperature and cannot even produce pure products, due to the characteristics of multicomponent system and large numbers of complex salts, such as $NaNO_3{\cdot}Na_2SO_4{\cdot}H_2O$, $Na_2SO_4{\cdot}3K_2SO_4$, $KCl{\cdot}MgCl_2{\cdot}6H_2O$, etc. [3–9].

✉ Xue-Li Huang
huangxueli@xju.edu.cn; 734078010@qq.com

[1] College of Chemistry and Chemical Engineering, Xinjiang University, Ürümqi 830046, People's Republic of China

[2] Key Laboratory of Cleaner Transition of Coal & Chemicals Engineering of Xinjiang Uyghur Autonomous Region, Ürümqi 830046, People's Republic of China

The solid–liquid phase equilibrium of a salt-water system is closely affected by temperature, especially for normal temperatures, and the phase diagrams are complex because of the presence of various double salts. For example, at 298 K, six, two and four types of double salts have been found in the Na^+, K^+, Mg^{2+}//Cl^-, SO_4^{2-}–H_2O system [6, 10], the Na^+, K^+//Cl^-, NO_3^-, SO_4^{2-}–H_2O system [6, 11], and the Na^+, K^+, Li^+// Cl^-, SO_4^{2-}–H_2O system [12], respectively. However, at a higher operating temperature, the crystallization regions of the double salts involving nitrate or magnesium chloride, such as $KCl{\cdot}MgCl_2{\cdot}6H_2O$ and $NaNO_3{\cdot}Na_2SO_4{\cdot}H_2O$, decrease or even disappear; at a lower temperature, a similar tendency could also be observed that crystallization zones of sulfate-type double salts, such as $Na_2SO_4{\cdot}3K_2SO_4$ and $K_2SO_4{\cdot}MgSO_4{\cdot}H_2O$, decrease or even disappear. All of the crystallization zones of sulfate-type double salts in these systems disappear when the temperature is below 298 K [13–15]. This indicates that the temperature has a strong influence on the crystallization behavior and the solubility of salts. The low-temperature treatments have some advantages in terms of fewer species of complex salts, high separation efficiency and purer final quality of salts products. Thus, the phase equilibria at low temperature are suitable for applications associated with crystallization and purification processes.

Currently, there are few reports in the aspect of the brine associated with Na^+, K^+, Mg^{2+}, Cl^-, NO_3^-, SO_4^{2-}, H_2O at low temperature. However, it can be speculated that the types of double salts involved in this multicomponent system diminish at low temperature, which could simplify the phase diagram relationship. Thus, an alternative route in terms of dealing with the brine, that is, a relatively simple low-temperature processing method, can be promoted. The cooling crystallization processes have proved to play an efficient role in some fields [16–22]. Accurate knowledge of the phase diagrams is thus essential at low temperatures.

To exploit the valuable brine resources economically, it is important to adopt the local natural conditions including low temperatures. The winter in salt lake areas is both long and cold, with an average temperature of 258 K, providing large cold capacity. So, the study of phase equilibrium at this temperature would have more practical significance to better guide salt lake production in winter.

The Na^+, K^+, Mg^{2+}//Cl^+, NO_3^-, SO_4^{2-}–H_2O system saturated with $NaCl{\cdot}2H_2O$ has four quinary subsystems at 258 K, which are necessary for studying the solid–liquid equilibrium of the complex six-component system. Among them, the quinary system Na^+, K^+, Mg^{2+}//Cl^-, NO_3^-–H_2O is an important system of natural brine type associated with nitrate deposits, also involved in other chemical processes or some industrial wastewater treatments, but the phase equilibrium of this system has not been reported so far. This quinary system saturated with NaCl contains three quaternary subsystems and eight ternary subsystems. Except for the solubilities of the quaternary subsystems Na^+, K^+, Mg^{2+}//Cl^-–H_2O, Na^+ and Mg^{2+}//Cl^-, NO_3^-–H_2O, those of other subsystems can be found in some compilations. The results show that the subsystems Na^+//Cl^-, NO_3^-, SO_4^{2-}–H_2O [13] and Na^+, K^+//Cl^-, NO_3^-, SO_4^{2-}–H_2O [14] are both of simple types without double salts, whereas the quinary subsystem Na^+, K^+, Mg^{2+}//Cl^-, SO_4^{2-}–H_2O [15] is of a complex type with the double salt $KCl{\cdot}MgCl_2{\cdot}6H_2O$ formed at 258 K.

In this paper, we will supply the solubility data of the Na^+, K^+, Mg^{2+}//Cl^-–H_2O and Na^+, K^+, Mg^{2+}//Cl^-, NO_3^-–H_2O systems; these data can be used as a theoretical reference for the design and optimize the process and is the basis for the utilization of brine resource.

Table 1 Chemical sample specifications

Chemical	CAS number	Source	Mass fraction purity[a]
NaCl	7647-14-5	Kermel Chemical reagent Co.,Ltd	0.99
KCl	7447-40-7	Kermel Chemical reagent Co.,Ltd	0.99
$NaNO_3$	7631-99-4	Kermel Chemical reagent Co.,Ltd	0.99
KNO_3	7757-79-1	Kermel Chemical reagent Co.,Ltd	0.99
$MgCl_2{\cdot}6H_2O$	7791-18-6	Tianjin First reagent Co.,Ltd	0.98
$Mg(NO_3)_2{\cdot}6H_2O$	13446-18-9	Tianjin First reagent Co.,Ltd	0.98

[a]All chemical reagents were used without further purification

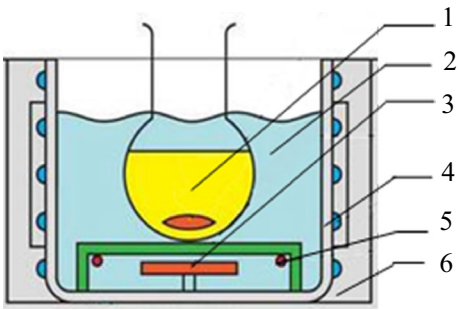

Fig. 1 Schematic illustration of experimental apparatus: 1. sample, 2. refrigerant, 3. stirring motor, 4. cooling coils, 5. heating tube, 6. stainless steel tank

2 Experimental Section

2.1 Reagents and Apparatus

The experimental materials were of analytical grade with purities not less than 98.0% mass fraction and all of them were used without any further purification. As tabulated in Table 1. NaCl, KCl, $NaNO_3$ and KNO_3 were purchased from the Chemical Reagent Factory of Tianjin Kermel, China, and were dried for 5–8 h at 105 °C prior to their use, the $MgCl_2{\cdot}6H_2O$ and $Mg(NO_3)_2{\cdot}6H_2O$ supplied by Tianjin First Reagent Corporation. Doubly distilled water (DDW) with an electrical conductivity less than 1.0×10^{-4} s·m^{-1} and pH of about 6.6 at room temperature was used.

A magnetically stirred thermostatic bath (DHJF-4010A, Zhengzhou Changcheng Instrument Co., Ltd., China), maintaining the temperature range from –40 to 99 °C with an accuracy of ± 0.1 °C, was employed for the equilibrium experiments, and its temperature control accuracy was calibrated using a precise thermometer. As presented in Fig. 1, the apparatus mainly included four parts: a stainless steel tank, the heating tube, the cooling coils and a stirring motor. An X-ray diffraction analyzer (D8 Advance, Bruker, Germany) was employed for solid phase characterization. Raman spectra(LabRAM HR Evolution, HORIBA Scientific, France) was recorded from 1000 to 4000 cm^{-1} using the 532 nm line from an argon ion laser at a power of 100 mW and am integration time of 30 s at the sample.

2.2 Experimental Procedure

The solubilities data of the systems were determined by means of the isothermal solution method in this study. The other third or fourth salt was added gradually to the initial samples until the quaternary or quinary system's invariant point was seen at 258 K. The appropriate salts and distilled water were mixed together and sealed in a 250 cm^3 glass bottle. Then the bottle was placed in the magnetic stirring thermostatic bath, which was set to the desired temperature. The magnetic stirrer in the bottom of flask worked at a fixed speed. Samples of the liquid phase were taken periodically for chemical analysis. It was assumed that equilibrium was achieved when the concentration of the solution remained constant. The experimental results showed that the equilibrium time for the three systems was at least 16 h. After equilibration, stirring was stopped, and the equilibrated system was allowed to rest for 3 h to ensure that the solid settled and the liquid cleared.

The liquid phases were taken out with a pre-cooled pipette at 258 K and transferred to a 250 mL volumetric flask and diluted for the measurement of the compositions by chemical or instrument analysis. The solid phases were identified by powder X-ray diffraction. By changing the amount of the salts and deionized water added, other points in the liquid and their equilibrium solids can be determined, thus allowing the phase diagram to be plotted. All of these were applied to the above systems.

2.3 Analytical Methods

The concentration of (Cl^-) was analyzed by 0.1 mol·L^{-1} $AgNO_3$ volumetric method with a precision of 0.3%; The (Mg^{2+}) ion concentration was determined by titration with an EDTA at pH = 9.0–10.0 (ammonia buffer) with the indicator Eriochrome Black-T with a standard uncertainty of less than 0.5%; The (K^+) ion concentration was measured by a gravimetric method (uncertainty of 0.2%), The (NO_3^-) ion concentration was analyzed by potassium dichromate oxidization (uncertainty of 0.6%). The (Na^+) ion concentration was evaluated from an ion balance.

3 Results and Discussion

3.1 Quaternary Homo-Ion System Na^+, K^+, Mg^{2+}//Cl^-–H_2O

The experimental data on the solubilities of the equilibrated solution and equilibrated solid phases in the quaternary system determined experimentally are given in Table 2.

As a quaternary conjugate salt system, the phase diagram of the quaternary system with a common anion can be represented by a trigonal prism as shown in Fig. 2. In this diagram, its three coordinates are $J(2Na^+)$, $J(2\ K^+)$ and $J(H_2O)$, respectively, which are respective Jänecke index values, and can be calculated according to the following correlations. The Jänecke index values were listed in Table 2.

The Jänecke indices were calculated using the following equations. Letting

$$[b] = \frac{1}{2} \times \frac{w(K^+)}{39.10} + \frac{1}{2} \times \frac{w(Na^+)}{22.99} + \frac{w(Mg^{2+})}{24.30} \quad (1)$$

Table 2 Solubilities data of the quaternary system Na^+, K^+, Mg^{2+}//Cl^-–H_2O at $T = 258$ K and 0.1MPa

No.	Composition of solution, 100*w*				Jänecke index J/[mol·(100 mol)$^{-1}$ ($2Na^+ + 2K^+ + Mg^{2+}$)]			Solid phase[a]
	Cl^-	Mg^{2+}	K^+	Na^+	$2Na^+$	$2K^+$	H_2O	
1,A_1	14.68	0.00	0.00	9.52	100.00	0.00	2032	Hy
2,A_2	25.25	8.65	0.00	0.01	0.00	0.00	1030	M_8
3,B_1	15.82	0.00	3.31	8.32	81.02	18.98	1805	Hy + KCl
4	15.88	0.84	2.92	6.99	67.95	16.69	1818	Hy + KCl
5	16.12	1.66	2.60	5.79	55.40	14.60	1803	Hy + KCl
6	16.23	1.97	2.45	5.36	50.94	13.69	1795	Hy + KCl
7	16.52	2.58	2.23	4.52	42.13	12.26	1767	Hy + KCl
8	17.11	3.26	1.81	3.87	34.86	9.58	1701	Hy + KCl
9	17.90	4.32	1.49	2.56	22.10	7.55	1621	Hy + KCl
10	18.51	4.85	1.24	2.10	17.58	6.05	1558	Hy + KCl
11	19.16	5.45	1.07	1.49	11.93	5.08	1497	Hy + KCl
12	20.08	6.20	0.84	0.80	6.10	3.79	1413	Hy + KCl
13,C_1	20.29	6.28	0.85	0.78	5.86	3.81	1393	Hy + KCl + Car
14	20.01	6.22	0.82	0.73	5.55	3.71	1421	Hy + Car
15	20.24	6.35	0.79	0.65	4.94	3.54	1400	Hy + Car
16	20.34	6.43	0.68	0.63	4.77	3.01	1392	Hy + Car
17	20.39	6.45	0.68	0.62	4.67	3.04	1387	Hy + Car
18	20.89	6.71	0.47	0.58	4.30	2.02	1344	Hy + Car
19	21.08	6.86	0.32	0.50	3.71	1.36	1330	Hy + Car
20,C_2	24.29	8.26	0.04	0.10	0.69	0.13	1090	Hy + Car + M_8
21,B_2	25.16	8.56	0.00	0.12	0.80	0.00	1035	Hy + M_8
22	24.22	8.29	0.02	0.01	0.08	0.09	1096	Car + M_8
23,B_3	23.92	8.18	0.05	0.01	0.00	0.19	1117	Car + M_8
24	20.25	6.39	0.83	0.56	4.28	3.73	1399	KCl + Car
25	19.95	6.44	0.81	0.28	2.14	3.70	1430	KCl + Car
26,B_4	20.05	6.61	0.84	0.00	0.00	3.81	1423	KCl + Car

Standard uncertainties *u* are $u(T) = 0.2$ K, $u(P) = 1$ kPa, $u_r[w(Cl^-)] = 0.003$, $u_r[w(Mg^{2+})] = 0.005$, and $u_r[w(K^+)] = 0.002$; *w* mass fraction

[a]Hy–$NaCl{\cdot}2H_2O$; Car–$KCl{\bullet}MgCl_2{\cdot}6H_2O$; M_8–$MgCl_2{\cdot}8H_2O$

$$J(2Na^+) = \frac{1}{2} \times \frac{w(Na^+)}{22.99[b]} \times 100 \tag{2}$$

$$J(2K^+) = \frac{1}{2} \times \frac{w(K^+)}{39.10[b]} \times 100 \tag{3}$$

$$J(H_2O) = \frac{w(H_2O)}{18.01[b]} \times 100 \tag{4}$$

where w(ion) or $w(H_2O)$ is the mass of the ion or water in g per 100 g of solution, respectively. J(ion) or $J(H_2O)$ are the Jänecke index values of the ion or water, respectively.

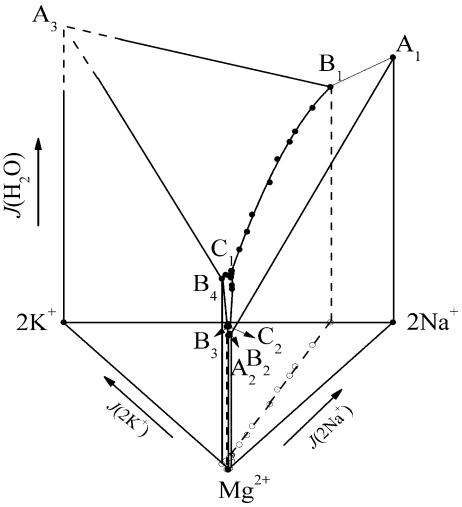

Fig. 2 Stereodiagram of the quaternary system Na^+, K^+, Mg^{2+}//Cl^-–H_2O at 258 K (the region near point A_3, where the KCl and ice are crystallized simultaneously at 258 K because of the low solubility and high eutectic temperature of the solution, was not investigated in this paper, therefore not plotted in proportion)

On the basis of the Jänecke index values in Table 2, the stereodiagram of the quaternary system Na^+, K^+, Mg^{2+}//Cl^-–H_2O at 258 K was plotted as shown in Fig. 2 and the planar projection of the phase diagram and the diagram of water contents are plotted in Figs. 3, 4 and 5.

The phase diagram is composed of two invariant points, five univariant curves, and six crystallized regions of single salts. Three vertices A_1, A_2, A_3 of the triangle represent salts of NaCl, $MgCl_2$ and KCl. B_1 and B_2 are the invariant points of ternary systems Na^+, K^+//Cl^-–H_2O, Na^+, Mg^{2+}//Cl^-–H_2O, at 258 K, respectively. The K^+, Mg^{2+}// Cl^-–H_2O ternary system at 258 K is a complex type with two invariant points of point B_3 and B_4. The invariant points of the quinary system are labeled as C_1 and C_2. The point C_1 is co-saturated with three salts $NaCl{\cdot}2H_2O + KCl + KCl{\cdot}MgCl_2{\cdot}6H_2O$ and an equilibrium solution with $w(Cl^-) = 20.29$ wt%, $w(Mg^{2+}) = 6.28$ wt%, and $w(K^+) = 0.85$ wt%. The point C_2 is co-saturated with three salts $NaCl{\cdot}2H_2O + MgCl_2{\cdot}8H_2O + KCl{\cdot}MgCl_2{\cdot}$

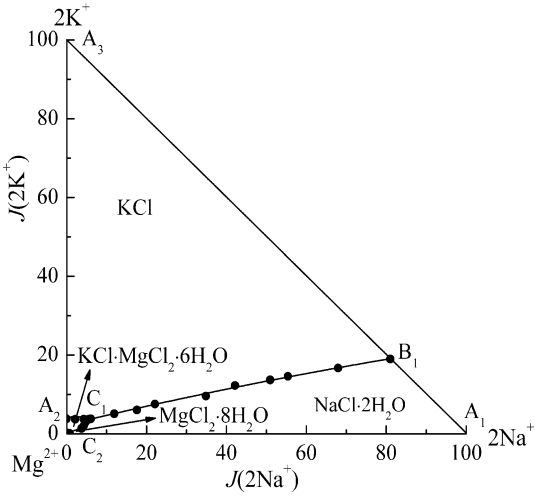

Fig. 3 Planar projection of the quaternary system Na^+, K^+, Mg^{2+}// Cl^-–H_2O at 258 K

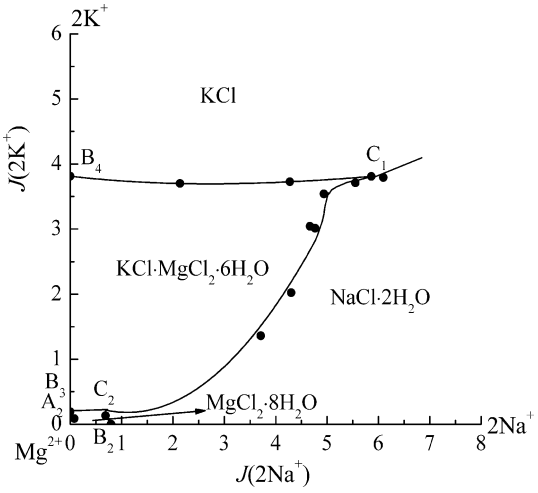

Fig. 4 Partial enlargement diagram of Fig. 3

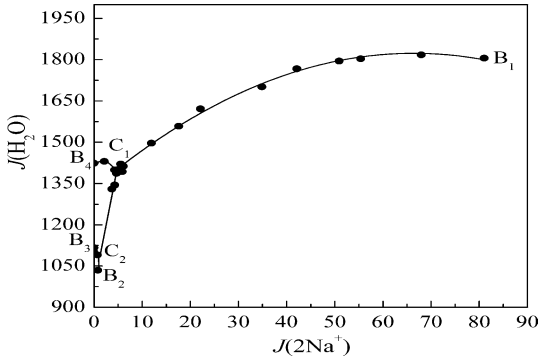

Fig. 5 Water-content diagram of the quaternary system Na^+, K^+, Mg^{2+}//Cl^-–H_2O at 258 K

$6H_2O$ and an equilibrium solution with $w(Cl^-) = 24.29$ wt%, $w(Mg^{2+}) = 8.26$ wt%, and $w(K^+) = 0.04$ wt%.

As shown in Fig. 6, the solids at two invariant points C_1 and C_2 were analyzed by X-ray diffraction, allowing the determination of the natures of the solid phases in equilibrium. The existence of the double salt $KCl{\cdot}MgCl_2{\cdot}6H_2O$ can be determined. The salts can form a hydrated phase, which is only stable in a particular temperature range, and melt with changes of the conditions. Magnesium chloride can be formed from various hydrated salts, including $MgCl_2{\cdot}12H_2O$, $MgCl_2{\cdot}8H_2O$ and $MgCl_2{\cdot}6H_2O$. The literature demonstrated the existence of the hydrate $MgCl_2{\cdot}12H_2O$ in the temperature range 239–256 K, $MgCl_2{\cdot}8H_2O$ at 256–269 K and $MgCl_2{\cdot}6H_2O$ at 273–389 K. The research on this system shows that $MgCl_2{\cdot}8H_2O$ is the crystallization form of magnesium chloride [5, 6, 23–26]. In addition, the literature [5, 6, 25–27] shows that at 258 K, sodium chloride can form hydrated ($NaCl{\cdot}2H_2O$) in binary or ternary systems. Besides, Raman microscopy makes it possible to determine precisely the salt hydrates that crystallize upon cooling [28, 29]. We measured the Raman spectra of various aqueous solutions at different temperatures and showed that $NaCl{\cdot}2H_2O$ exists in the systems at 258 K, consistent with the literature.

It is worth mentioning that, compared to the phase studies at higher temperature, studies at 258 K are more difficult, the salts can form various hydrated salts and the

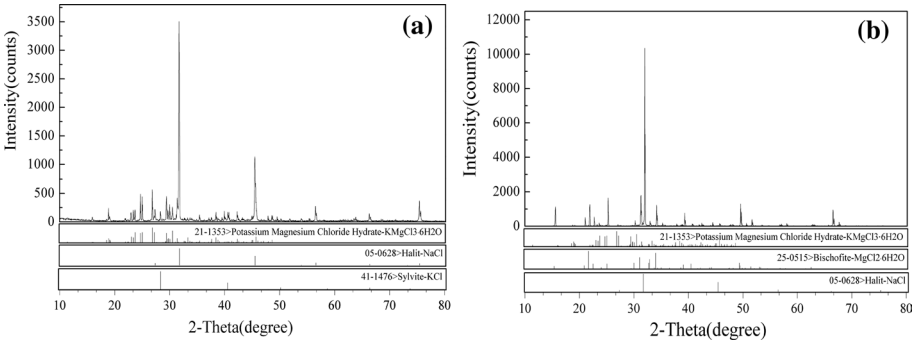

Fig. 6 X-ray diffraction patterns of the solid phases in the invariant point of **a** C_1, **b** C_2 of the quaternary system Na^+, K^+, Mg^{2+}//Cl^-–H_2O at 258 K

solutions have greater viscosity, which increases the complexity of the study on the phase equilibrium. Besides, because hydrate phases are only stable in special temperature and pressure ranges, they melt with the change of conditions. The limitation of experimental and equipment conditions, $MgCl_2{\cdot}8H_2O$ and $NaCl{\cdot}2H_2O$ were difficult to detect by X-ray diffraction. So, in Figs. 7 and 12, the X-ray diffraction patterns of the invariant points consist of $MgCl_2{\cdot}6H_2O$ and NaCl, instead of $MgCl_2{\cdot}8H_2O$ and $NaCl{\cdot}2H_2O$.

The salts corresponding to the five-univariant curves B_1C_1, B_4C_1, C_1C_2, B_3C_2 and B_2C_2 are $NaCl{\cdot}2H_2O + KCl$, $KCl{\cdot}MgCl_2{\cdot}6H_2O + KCl$, $KCl{\cdot}MgCl_2{\cdot}6H_2O + NaCl{\cdot}2H_2O$, $KCl{\cdot}MgCl_2{\cdot}6H_2O + MgCl_2{\cdot}8H_2O$ and $MgCl_2{\cdot}8H_2O + NaCl{\cdot}2H_2O$, respectively.

The four crystallization fields correspond to three single salts $NaCl{\cdot}2H_2O$, KCl, $MgCl_2{\cdot}8H_2O$, and one double salts $KCl{\cdot}MgCl_2{\cdot}6H_2O$. The crystallization area of $MgCl_2{\cdot}8H_2O$ occupies the smallest part because of its high solubility. Whereas the crystallization areas of KCl and $NaCl{\cdot}2H_2O$ are larger, which indicates that they are more easily saturated and crystallize out from the solution in this system as a result of the strong salting-out effect of other salts.

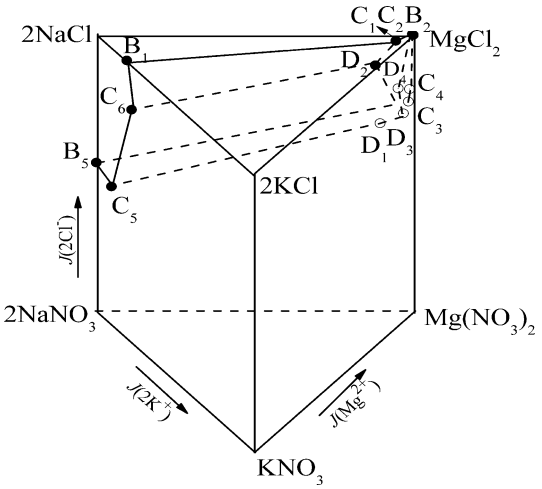

Fig. 7 The crystallization region of $NaCl{\cdot}2H_2O$ in the phase diagram of the quinary system Na^+, K^+, Mg^{2+}//Cl^-, NO_3^-–H_2O at 258 K (only invariant points)

The water-content diagram is essential for the design and calculation of crystallization processes. As shown in Fig. 5, with $J(2Na^+)$ as the abscissa, and $J(H_2O)$ as the ordinate, we can see that at the univariant curves B_1C_1, B_2C_1 and C_1C_2, the water content changes obviously, while at the other univariant curves, the water content changes slightly, which can be explained by the increase of the mass fraction of $MgCl_2$. On the univariant curve B_1C_1, $J(H_2O)$ increases to a maximum value with the decreasing of $J(2Na^+)$ and then decreases with further reduction of $J(2Na^+)$.

4 Quinary System $Na^+, K^+, Mg^{2+}//Cl^-, NO_3^-–H_2O$

Findings obtained from our previous research show that, NaCl should crystallize first from the solution during the cooling process because of the high concentration of NaCl in actual nitrate brine. So, the phase diagrams on the condition saturated with $NaCl·2H_2O$ at low temperatures have more practical value. Besides, the equilibrium of the quinary system is beneficial to the construction of the phase diagrams of the complex six-component system.

The measured solubilities data of the quinary system Na^+, K^+, $Mg^{2+}//Cl^-$, $NO_3^-–H_2O$ saturated with $NaCl·2H_2O$ are presented in Tables 3 and 4. The concentration of each ion is expressed in mass fraction.

Na^+, K^+, $Mg^{2+}//Cl^-$, $NO_3^-–H_2O$ is a complicated quinary system, the isothermal phase behavior of which has four dimensions. The solvent-less projection (the dry salt phase diagram) obtained by elimination of the solvent coordinate decreases the dimensionality to three and can be represented in form of a trigonal prism as shown in Fig. 8, the coordinates of which are the Jänecke index $J(2\ K^+)$, $J(Mg^{2+})$ and $J(2Cl^-)$ respectively. These Jänecke index can be calculated according to the following equations and listed in Table 3.

Letting

$$[M] = \frac{1}{2} \times \left(\frac{w(Cl^-)}{35.45} + \frac{w(NO_3^-)}{62.00} \right) \tag{5}$$

$$J(2K^+) = \frac{1}{2} \times \frac{w(K^+)}{39.10[M]} \times 100 \tag{6}$$

$$J(Mg^{2+}) = \frac{w(Mg^{2+})}{24.31[M]} \times 100 \tag{7}$$

$$J(2Cl^-) = \frac{1}{2} \times \frac{w(2Cl^-)}{35.45[M]} \times 100 \tag{8}$$

$$J(H_2O) = \frac{w(H_2O)}{18.01[M]} \times 100 \tag{9}$$

According to the Jänecke index in Table 3, the crystallization space of $NaCl·2H_2O$ can be plotted in Fig. 7, which has four invariant points saturated with $NaCl·2H_2O$ and other three salts, nine univariant curves saturated with $NaCl·2H_2O$ and other two salts, and six crystallization fields saturated with $NaCl·2H_2O$ and the other salts.

Table 3 Solubilities data of the quinary system Na^+, K^+, Mg^{2+}//Cl^-, NO_3^-–H_2O saturated with $NaCl{\cdot}2H_2O$ at $T = 258$ K and 0.1 MPa

No	Composition of solution, 100*w*					Jänecke index J/[mol·(100 mol)$^{-1}$ ($2Cl^- + 2NO_3^-$)]				Solid phase[a]
	NO_3^-	Cl^-	K^+	Mg^{2+}	Na^+	Mg^{2+}	2 K^+	$2Cl^-$	H_2O	
1,C_5	17.41	9.88	2.06	0.00	11.66	0.00	9.39	49.82	1171	Hy + NN + KN
2	16.80	10.41	2.00	0.51	10.84	7.48	9.05	52.01	1169	Hy + NN + KN
3	15.64	10.63	1.84	1.05	9.63	15.61	8.54	54.31	1231	Hy + NN + KN
4	15.19	11.20	1.80	1.28	9.42	18.81	8.22	56.32	1210	Hy + NN + KN
5	14.29	11.67	1.69	1.75	8.57	25.66	7.72	58.82	1231	Hy + NN + KN
6	13.07	12.12	1.50	2.45	7.19	36.44	6.95	61.86	1279	Hy + NN + KN
7	11.90	12.61	1.36	3.04	6.04	45.62	6.37	64.95	1319	Hy + NN + KN
8	10.99	13.50	1.23	3.63	5.24	53.54	5.64	68.24	1301	Hy + NN + KN
9	10.22	14.01	1.13	4.23	4.21	62.10	5.17	70.57	1312	Hy + NN + KN
10	9.84	14.53	1.00	4.80	3.40	69.43	4.51	72.10	1297	Hy + NN + KN
11	9.24	15.81	0.81	5.94	1.97	82.10	3.48	74.95	1236	Hy + NN + KN
12,D_1	9.36	16.64	0.71	6.63	1.30	87.90	2.93	75.67	1170	Hy + NN + KN + Nit
13	10.05	17.16	0.67	7.17	0.90	91.29	2.64	74.91	1101	Hy + NN + Nit
14	10.36	17.60	0.36	7.64	0.59	94.78	1.39	74.82	1062	Hy + NN + Nit
15	9.66	19.00	0.15	8.13	0.43	96.76	0.55	77.47	1005	Hy + NN + Nit
16,C_3	9.44	18.66	0.00	8.08	0.31	97.97	0.00	77.57	1039	Hy + NN + Nit
17,C_6	4.91	14.49	4.21	0.00	8.74	0.00	22.05	83.78	1540	Hy + KN + Sy
18	4.61	14.80	3.99	0.41	8.19	6.81	20.75	84.89	1535	Hy + KN + Sy
19	4.57	14.84	3.91	0.82	7.47	13.73	20.29	85.04	1543	Hy + KN + Sy
20	4.40	14.93	3.69	1.04	7.18	17.37	19.10	85.57	1551	Hy + KN + Sy
21	4.08	15.22	3.50	1.53	6.43	25.43	18.08	86.71	1553	Hy + KN + Sy
22	3.99	15.42	3.25	1.87	6.03	30.87	16.63	87.11	1544	Hy + KN + Sy
23	3.80	15.50	3.10	2.30	5.29	37.92	15.89	87.71	1560	Hy + KN + Sy
24	3.65	15.84	2.81	2.72	4.83	44.24	14.19	88.35	1540	Hy + KN + Sy
25	3.41	16.04	2.54	3.18	4.16	51.61	12.79	89.15	1546	Hy + KN + Sy
26	3.12	16.74	2.16	3.93	3.31	61.84	10.56	90.38	1503	Hy + KN + Sy
27	3.06	17.47	1.88	4.59	2.68	69.61	8.86	90.90	1440	Hy + KN + Sy
28	2.96	17.87	1.67	5.12	2.02	76.32	7.72	91.34	1415	Hy + KN + Sy
29,D_2	2.82	18.78	1.37	5.91	1.24	84.57	6.09	92.10	1349	Hy + KN + Sy + Car
30	2.97	19.18	1.21	6.31	0.89	88.13	5.27	91.87	1309	Hy + Sy + Car
31	1.93	18.60	1.24	6.01	0.68	88.98	5.69	94.39	1429	Hy + Sy + Car
32	1.43	20.28	1.02	6.27	1.22	86.72	4.39	96.13	1302	Hy + Sy + Car
33	1.07	19.50	1.10	6.15	0.76	89.26	4.94	96.97	1398	Hy + Sy + Car
34,C_1	0.00	20.24	0.79	6.35	0.65	91.50	3.54	100.00	1400	Hy + Sy + Car
35	4.01	19.13	1.17	6.56	0.79	89.36	4.94	89.29	1256	Hy + KN + Car
36	4.83	18.62	0.86	6.51	1.04	88.84	3.64	87.07	1254	Hy + KN + Car
37	5.37	18.25	0.80	6.41	1.23	87.74	3.39	85.59	1254	Hy + KN + Car
38,D_3	9.67	18.03	0.42	7.72	0.43	95.64	1.60	76.53	1065	Hy + KN + Car + Nit
39	8.65	19.25	0.18	8.04	0.37	96.96	0.67	79.57	1033	Hy + Car + Nit
40	9.05	20.17	0.13	8.45	0.37	97.26	0.47	79.58	960.0	Hy + Car + Nit
41	8.81	19.79	0.11	8.33	0.28	97.85	0.41	79.71	993.8	Hy + Car + Nit
42,D_4	8.52	20.34	0.15	8.36	0.45	96.77	0.55	80.67	970.7	Hy + Car + Nit + M_8

Table 3 (continued)

No	Composition of solution, 100*w*					Jänecke index J/[mol·(100 mol)$^{-1}$ ($2Cl^- + 2NO_3^-$)]				Solid phase[a]
	NO_3^-	Cl^-	K^+	Mg^{2+}	Na^+	Mg^{2+}	2 K^+	$2Cl^-$	H_2O	
43,C_4	8.66	20.01	0.00	8.42	0.26	98.36	0.00	80.17	988.0	Hy + Nit + M_8
44	7.48	20.85	0.10	8.44	0.27	97.99	0.35	82.97	984.6	Hy + Car + M_8
45	5.11	21.24	0.16	8.16	0.14	98.50	0.59	87.91	1062	Hy + Car + M_8
46	2.25	24.59	0.04	8.85	0.01	99.79	0.14	95.03	977.4	Hy + Car + M_8
47	1.67	25.07	0.05	8.81	0.18	98.81	0.19	96.34	971.4	Hy + Car + M_8
48	1.42	24.16	0.07	8.41	0.24	98.28	0.26	96.75	1035	Hy + Car + M_8
49	0.85	23.38	0.07	7.93	0.43	96.98	0.28	97.97	1111	Hy + Car + M_8
50,C_2	0.00	24.29	0.04	8.26	0.10	99.19	0.13	100.00	1091	Hy + Car + M_8
51,B_5	15.29	10.14	0.00	0.00	12.25	0.00	0.00	53.70	1299	Hy + NN
52,B_2	0.00	25.16	0.00	8.56	0.12	99.25	0.00	100.00	1035	Hy + M_8
53,B_1	0.00	15.82	3.31	0.00	8.32	0.00	18.98	100.00	1805	Hy + Sy

Standard uncertainties u are $u(T) = 0.2$ K, $u(P) = 1$ kPa, $u_r[w(K^+)] = 0.002$, $u_r[w(Cl^-)] = 0.003$, $u_r[w(Mg^{2+})] = 0.005$, and $u_r[w(NO_3^-)] = 0.006$

w mass fraction

[a]Hy–$NaCl{\cdot}2H_2O$; KN–KNO_3; Sy–KCl; NN–$NaNO_3$; M_8–$MgCl_2{\cdot}8H_2O$; Nit–$Mg(NO_3)_2{\cdot}6H_2O$; and Car–$KCl{\cdot}MgCl_2{\cdot}6H_2O$

Figure 7 is a stereodiagram and not easy to apply. The Cl-less projection (planar projection diagram) obtained by deducting the variable of Cl can reduce the dimension to two, and be plotted in a 2-D figure as shown in Figs. 8 and 9, the two coordinates of which are $J(Mg^{2+})$ and $J(2\ NO_3^-)$; The water and contents of Cl can be indicated by the water-content diagram and chlorine-content diagrams respectively as shown in Figs. 10 and 11, the two coordinates of which are $J(Mg^{2+})$ and $J(H_2O)$, $J(Mg^{2+})$ and $J(Cl^-)$. These Jänecke indices are listed in Table 4.

As shown in Table 4 and Figs. 8, 9, 10 and 11, the quinary system Na^+, K^+, Mg^{2+}// Cl^-, NO_3^-–H_2O is of a complex type, with the double salt $KCl{\cdot}MgCl_2{\cdot}6H_2O$ formed at 258 K, the phase diagram of which contains four invariant points, nine univariant curves, and six crystallization fields.

Each vertex B_1, B_2 and B_5 represents the invariant points of NaCl–KCl, $MgCl_2$–NaCl, and $NaNO_3$–NaCl salts in water at 258 K, respectively. The points C_1, C_2, C_3, C_4, C_5, and C_6 on the sides correspond to the invariant points of quarternary subsystems Na^+, K^+, Mg^{2+}//Cl^-–H_2O, Na^+, Mg^{2+}//Cl^-, NO_3^-–H_2O, and Na^+, K^+//Cl^-, NO_3^-–H_2O respectively.

The points D_1, D_2, D_3 and D_4 are invariant points of the quinary system Na^+, K^+, Mg^{2+}//Cl^-, NO_3^-–H_2O. The mass fraction compositions of the corresponding equilibrated solution and equilibrated solids of D_1, D_2, D_3 and D_4 are listed as follows.

Point D_1 is analyzed as 9.36% mass (NO_3^-), 16.64% mass (Cl^-), 0.71% mass (K^+), 6.63% mass (Mg^{2+}), and co-saturated with salts $NaCl{\cdot}2H_2O$, $NaNO_3$, KNO_3 and $Mg(NO_3)_2{\cdot}6H_2O$.

Point D_2 is analyzed as 2.82% mass (NO_3^-), 18.78% mass (Cl^-), 1.37% mass (K^+), 5.91% mass (Mg^{2+}), and co-saturated with salts $NaCl{\cdot}2H_2O$, KCl, KNO_3 and $KCl{\cdot}MgCl_2{\cdot}6H_2O$.

Table 4 Jänecke index J [mol·(100 mol)$^{-1}$ (2 $K^+ + NO_3^- + Mg^{2+}$)] data of the quinary system Na^+, K^+, $Mg^{2+}//Cl^-$, NO_3^-–H_2O saturated with NaCl·$2H_2O$ at $T = 258$ K

No.	Mg^{2+}	$2NO_3^-$	$2Cl^-$	H_2O	No	Mg^{2+}	$2NO_3^-$	$2Cl^-$	H_2O
1,C_5	0.00	84.23	83.63	1965	28	82.33	9.34	98.56	1527
2	11.58	74.39	80.59	1812	29,D_2	85.81	8.01	93.44	1369
3	22.34	65.42	77.75	1763	30	86.80	8.01	90.49	1289
4	26.60	61.77	79.67	1710	31	88.73	5.59	94.13	1425
5	34.41	55.23	78.88	1651	32	91.30	4.07	101.18	1371
6	44.69	46.78	75.86	1568	33	91.81	3.12	99.74	1438
7	52.42	40.27	74.63	1515	34,C_1	96.28	0.00	105.19	1473
8	58.88	34.92	75.04	1431	35	85.10	10.20	85.07	1196
9	64.22	30.43	72.99	1357	36	84.29	12.26	82.63	1190
10	68.17	27.40	70.81	1274	37	83.13	13.65	81.12	1188
11	74.22	22.64	67.74	1117	38,D_3	79.23	19.44	63.41	882.23
12,D_1	76.33	21.13	65.71	1016	39	82.12	17.31	67.38	875.26
13	76.71	21.07	62.94	925.00	40	82.32	17.28	67.37	812.46
14	78.11	20.75	61.65	875.09	41	82.54	17.11	67.24	838.32
15	80.74	18.80	64.66	838.61	42,D_4	82.96	16.57	69.18	832.19
16,C_3	81.37	18.63	64.43	863.09	43,C_4	83.22	16.78	67.82	836.03
17,C_6	0.00	42.39	218.92	4023	44	84.94	14.76	71.92	853.59
18	15.97	35.41	198.94	3597	45	88.60	10.87	79.09	955.34
19	28.03	30.54	173.54	3150	46	95.13	4.738	90.60	931.78
20	34.08	28.31	167.84	3044	47	96.25	3.568	93.85	946.13
21	44.77	23.41	152.69	2733	48	96.55	3.196	95.05	1017
22	51.12	21.34	144.27	2556	49	97.67	2.043	98.67	1119
23	57.37	18.59	132.72	2359	50,C_2	99.87	0.00	100.69	1098
24	63.13	16.63	126.07	2197	51,B_5	0.00	100.00	115.89	2806
25	68.59	14.42	118.45	2055	52,B_2	100.00	0.00	100.80	1043
26	75.40	11.73	110.23	1833	53,B_1	0.00	0.00	527.19	9517
27	79.49	10.40	103.77	1645					

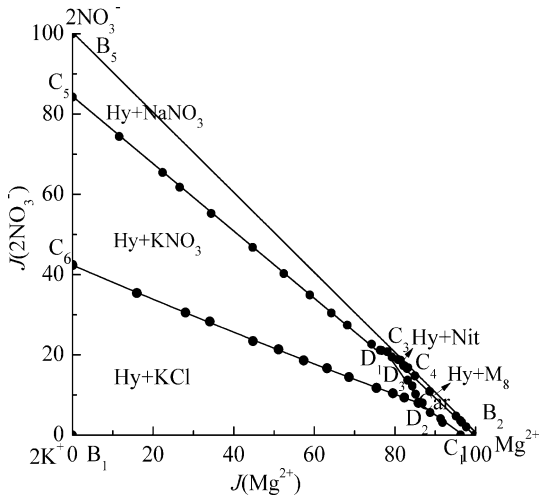

Fig. 8 Planar projection diagram of the quinary system Na^+, K^+, $Mg^{2+}//Cl^-$, NO_3^-–H_2O at 258 K saturated with NaCl·$2H_2O$

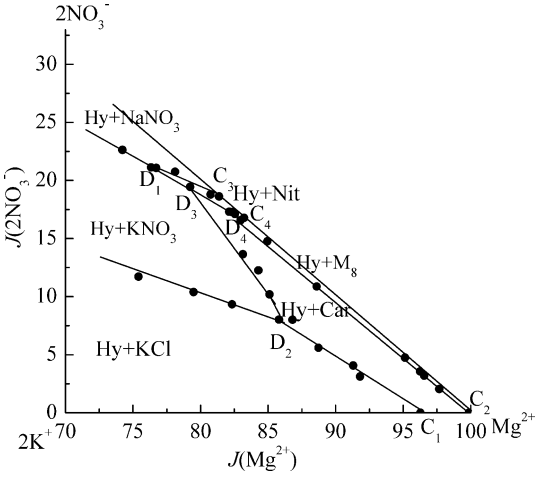

Fig. 9 Partial enlargement diagram of Fig. 8

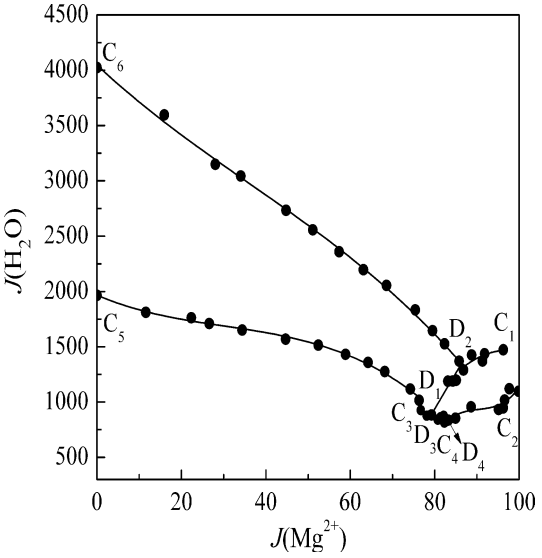

Fig. 10 Water-content diagram of the quinary Na^+, K^+, Mg^{2+}// Cl^-, NO_3^-–H_2O at 258 K saturated with $NaCl{\cdot}2H_2O$

Point D_3 is analyzed as 9.67% mass (NO_3^-), 18.03% mass (Cl^-), 0.42% mass (K^+), 7.72% mass (Mg^{2+}), and co-saturated with salts $NaCl{\cdot}2H_2O$, KNO_3, $KCl{\cdot}MgCl_2{\cdot}6H_2O$ and $Mg(NO_3)_2{\cdot}6H_2O$.

Point D_4 is analyzed as 8.52% mass (NO_3^-), 20.34% mass (Cl^-), 0.15% mass (K^+), 8.36% mass (Mg^{2+}), and co-saturated with salts $NaCl{\cdot}2H_2O$, $KCl{\cdot}MgCl_2{\cdot}6H_2O$, $MgCl_2{\cdot}8H_2O$, and $Mg(NO_3)_2{\cdot}6H_2O$.

Figure 12 shows the X-ray diffraction patterns corresponding to the equilibrium solid phases of the invariant points D_1, D_2, D_3 and D_4, respectively. The XRD spectra in Fig. 12 can only determine that $MgCl_2{\cdot}6H_2O$ and NaCl, in the solid phases, as a result of the limitations of sample and testing conditions. It is very difficult to find $MgCl_2{\cdot}8H_2O$ and $NaCl{\cdot}2H_2O$.

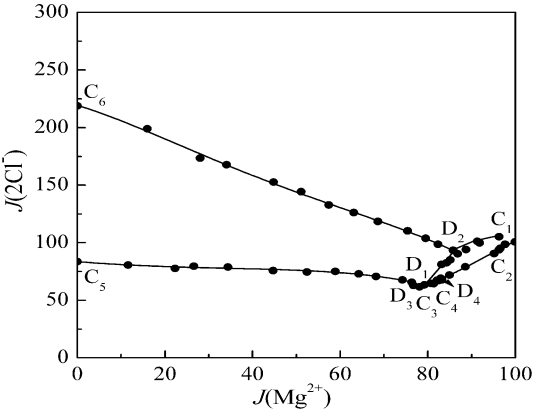

Fig. 11 Chlorine-content diagram of the quinary Na^+, K^+, Mg^{2+}//Cl^-, NO_3^-–H_2O at 258 K saturated with $NaCl{\cdot}2H_2O$

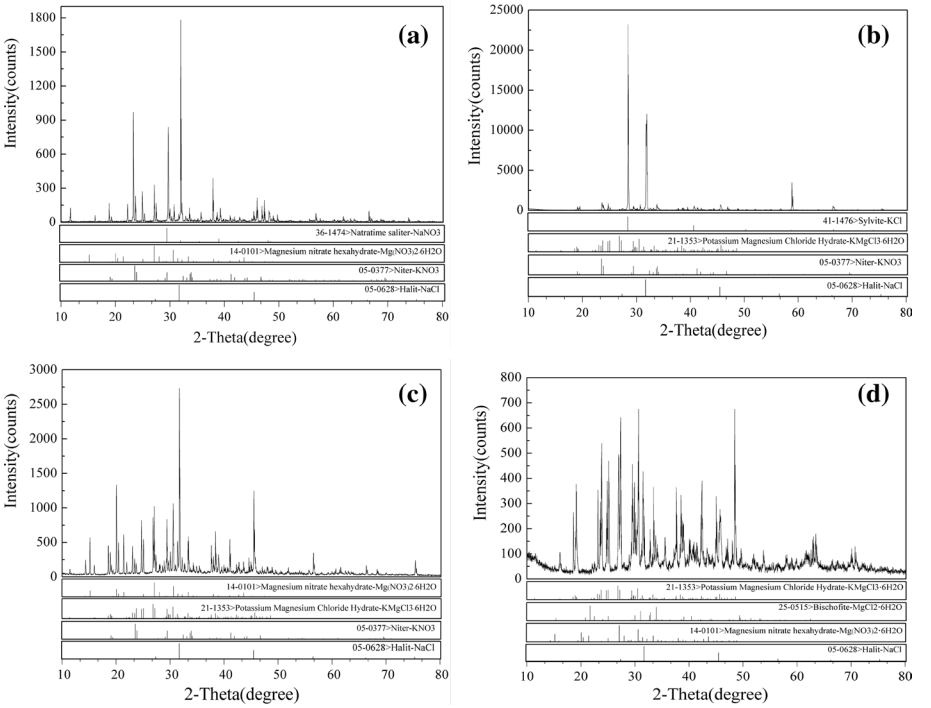

Fig. 12 X-ray diffraction patterns of the solid phases in the invariant point of **a** D_1, **b** D_2, **c** D_3 and **d** D_4 of the quinary system Na^+, K^+, Mg^{2+}//Cl^-, NO_3^-–H_2O at 258 K saturated with $NaCl{\cdot}2H_2O$

The nine univariant curves, C_5D_1, C_3D_1, D_1D_3, C_4D_4, D_3D_4, D_2D_3, C_6D_2, C_1D_2 and C_2D_4, are co-saturated with $NaCl{\cdot}2H_2O$ and two other salts, respectively.

The quinary phase diagram has six crystallization fields saturated with $NaCl{\cdot}2H_2O$ and another salt, the second salts being $NaNO_3$ ($B_5C_5D_1C_3$ field), KNO_3 ($C_5C_6D_2D_3D_1$ field), KCl ($C_6B_1C_1D_2$ field), $Mg(NO_3)_2{\cdot}6H_2O$ ($C_3D_1D_3D_4C_4$ field), $KCl{\cdot}MgCl_2{\cdot}6H_2O$ ($C_1D_2D_3D_4C_2$ field), and $MgCl_2{\cdot}8H_2O$ ($C_2\ D_4C_4\ B_2$ field).

It can be seen that the areas of the crystallization zones saturated with $NaCl{\cdot}2H_2O$ decrease in the order of KCl, KNO_3, $NaNO_3$, $KCl{\cdot}MgCl_2{\cdot}6H_2O$, $MgCl_2{\cdot}8H_2O$, $Mg(NO_3)_2{\cdot}6H_2O$. Among them, KNO_3 and KCl have larger crystallization areas and lower solubility than the other salts. This means that separation processes from the mixture solutions for the two salts are feasible due to their relatively large areas of crystallization. The fields of $Mg(NO_3)_2{\cdot}6H_2O$ and $MgCl_2{\cdot}8H_2O$ are extremely small, which are the result of their high solubility.

Figure 10 shows that the water-contents for the invariant points decrease apparently from D_2–D_1–D_3 to D_4, reaching the $J(H_2O)$ values of 832.19 mol·(100 mol)$^{-1}$ (2 $K^+ + 2NO_3^- + Mg^{2+}$) at the invariant point D_4. It can be concluded that the point D_4 has the highest concentration in the quinary system. The water content gradually decreases at the univariant curves C_6D_2 and it is almost unchanged at the univariant curves C_1D_2, C_2D_4 with increasing of the Jänecke index values of $J(Mg^{2+})$. The high concentration of Mg^{2+} ion in the quinary system implies that Mg^{2+} has a strong salting-out effect on other salts, which can decrease the solubilities of the other salts.

Figure 11 indicates that the chlorine-content of the points C_3, C_4, D_1, D_3 and D_4 are similar, about 65–70 mol·(100 mol)$^{-1}$ (2 $K^+ + NO_3^- + Mg^{2+}$); The lowest contents of Cl is at point D_3; The concentration of magnesium and nitrate ion significantly influence the chlorine content, especially on univariant curves C_6D_2, $C_1D_2D_3$ and C_2D_4. It clearly shows that the regularity in the variation of the chlorine content related to the $J(Mg^{2+})$ is a feature similar to that of the water content. The point D_4 possess the lowest water content, which is because of the higher solubility of $MgCl_2$ and $Mg(NO_3)_2$ compared to other salts at 258 K.

5 Conclusions

The phase equilibria of the quinary system Na^+, K^+, Mg^{2+}//Cl^-, NO_3^-–H_2O and the quaternary system Na^+, K^+, Mg^{2+}//Cl^-–H_2O have been investigated by the method of isothermal solution saturation. The results demonstrated that the quinary system Na^+, K^+, Mg^{2+}//Cl^-, NO_3^-–H_2O saturated with $NaCl{\cdot}2H_2O$ at 258 K belongs to a complex type, which contains four invariant points, nine univariant curves, and six crystallization fields. The salts $Mg(NO_3)_2{\cdot}6H_2O$ and $MgCl_2{\cdot}8H_2O$ have smaller crystallization areas and higher solubility than the other salts, so they are more difficult to separate from the solution in this system at the research temperature. The concentrations of Mg^{2+} and NO_3^- in the solution are the main factors affecting the water content and solution density. The findings of this study can be applicable in various industrial salts recovering units.

Acknowledgements The authors greatly acknowledge the financial support from the program of the National Natural Science Foundation of China (Grant No. 21766033) and the foundation of Key Laboratory of Cleaner Transition of Coal & Chemicals Engineering of Xinjiang University.

References

1. Zheng, M.P.: On saline lakes of China. Miner. Dep. **20**, 181–189 (2001)
2. Zhang, B.Q.: Present status of development and utilization of nitrate resources and its development prospect in China. Ind. Miner. Proces. **36**, 1–5 (2007)
3. Steiger, M.: The geochemistry of nitrate deposits : I. Thermodynamics of Mg $(NO_3)_2$–H_2O and solubilities in the Na^+–Mg^{2+}–NO_3^-–SO_4^{2-}–H_2O system. Chem. Geol. **36**, 84–97 (2016)

4. Chan, C.K., Liang, Z., Zheng, J., Clegg, S.L., Brimblecombe, P.: Thermodynamic properties of aqueous aerosols to high supersaturation: I–Measurements of water activity of the system Na^+–Cl^-–NO_3^-–SO_4^{2-}–H_2O at 298.15 K. Aerosol. Sci. Technol. **27**, 324–344 (1997)
5. Weast, R.C., Astle, M.J., Beyer, W.H.: CRC handbook of Chemistry and Physics. CRC Press, Boca Raton (1983)
6. Howard, S., Silcock, H.L.: Solubililies of Inorganic and Organic Compounds, 3rd edn. Pergamon Press, New York (1979)
7. Huang, X.L., Song, P.S., Chen, L.J., Lu, B.L.: Liquid–solid equilibria in quinary system Na^+, Mg^{2+}//Cl^-,SO_4^{2-}–NO_3^-–H_2O at 298.15 K. Calphad **32**, 188–194 (2008)
8. Huang, X.L., Zhu, L.J., Liang, T., Song, P.S.: Study on the phase equilibrium for the quinary system Na^+, K^+, Mg^{2+}//Cl^-,NO_3^-–H_2O at 298.16 K. Acta Chim. Sinica **65**, 798–802 (2007)
9. Yang, J., Wang, Y.F., Shu, M., Yang, L.B., Zhu, L., Zhao, X.Y., Shan, Z.L.: Solid–liquid equilibrium of quaternary system Na^+//Cl^-,–NO_3^-–SO_4^{2-}–H_2O at 373.15 K. Fluid Phase Equilib. **445**, 7–13 (2017)
10. Jin, Z.M., Xiao, X.Z., Liang, S.M.: Study of the metastable equilibrium for pentanary system of (Na^+, K^+, Mg^{2+}), (Cl–, SO_4^{2-}), H_2O. Acta Chim. Sin. **38**, 313–321 (1980)
11. Zhou, T., Wang, X.F., Huang, X.L., Li, H., Liu, N.: Liquid–solid metastable equilibria of a quinary system Na^+, K^+//Cl^-,SO_4^{2-},NO_3^-–H_2O at 298 K. J. Chem. Eng **29**, 510–515 (2015)
12. Song, P.S., Dong, Y.P., Wu, L.: The phase diagram of Li^+, Na^+, K^+//Cl–,SO_4^{2-}–H_2O quinary system at 25 °C and its application. J. Salt Lake Res. **25**, 9–17 (2017)
13. Zhang, X., Huang, X.L.: Study on the phase equilibria of the quaternary system Na^+//Cl–, NO_3^-, SO_4^{2-}–H_2O at low temperatures. Chemistry **78**, 337–341 (2015)
14. Liao, L., Huang, X.L., Song, H.: Phase equilibria of quinary system Na^+, K^+//Cl^-, SO_4^{2-}, NO_3^-–H_2O at 258.15 K. J. Chem. Eng. **30**, 7–12 (2016)
15. Zhu, Q.L., Huang, X.L.: Liquid-solid phase equilibrium of Na^+, K^+, Mg^{2+}//Cl–, SO_4^{2-}–H_2O system at −15°C. J. Chem. Ind. Eng. **66**, 1252–1257 (2015)
16. Ham, F.V.D., Witkamp, G.J., Graauw, J.D., Van Rosmalen, G.M.: Eutectic freeze crystallization simultaneous formation and separation of two solid phases. J. Cryst. Growth **198**, 744–748 (1999)
17. Kim, D.H.: A review of desalting process techniques and economic analysis of the recovery of salts from retentates. Desalination **270**, 1–8 (2011)
18. Mahdavi, M., Mahvi, A.H., Nasseri, S., Yunesian, M.: Application of freezing to the desalination of saline water. J. Sci. Eng. **36**, 1171–1177 (2011)
19. Hasan, M., Rotich, N., John, M., Louhi-Kultanen, M.: Salt recovery from wastewater by air-cooled eutectic freeze crystallization. Chem. Eng. J. **326**, 192–200 (2017)
20. Rich, A., Mandri, Y., Mangin, D., Rivoire, A., Abderafi, S.: Sea water desalination by dynamic layer melt crystallization: parametric study of the freezing and sweating steps. J. Cryst. Growth **342**, 110–116 (2012)
21. Vaessen, R., Seckler, M., Witkamp, G.J.: Eutectic freeze crystallization with an aqueous KNO_3–HNO_3 solution in a 100-L cooled-disk column crystallizer. Ind. Eng. Chem. Res. **42**, 4874–4880 (2003)
22. Hasan, M., Filimonov, R., Chivavava, J., Sorvari, J., Louhi-Kultanen, M., Lewis, A.E.: Ice growth on the cooling surface in a jacketed and stirred eutectic freeze crystallizer of aqueous Na_2SO_4 solutions. Sep. Purif. Technol. **175**, 512–526 (2017)
23. Christov, C.: Chemical equilibrium model of solution behavior and bishofite ($MgCl_2{\cdot}6H_2O$(cr)) and hydrogen-carnallite ($HCl{\cdot}MgCl_2{\cdot}7H_2O$(cr)) solubility in the $MgCl_2$+H_2O and $HCl{\cdot}MgCl_2$+H_2O systems to high acid concentration at (0 to 100) °C. J. Chem. Eng. Data **54**, 2599–2608 (2009)
24. Christov, C.: Isopiestic determination of the osmotic coefficients of an aqueous $MgCl_2$ + $CaCl_2$ mixed solution at (25 and 50)° C. Chemical equilibrium model of solution behavior and solubility in the $MgCl_2$ + H_2O and $MgCl_2$ + $CaCl_2$ + H_2O systems to high concentration at (25 and 50)°C. J. Chem. Eng. Data **54**, 627–635 (2008)
25. Pabalan, R.T., Pitzer, K.S.: Thermodynamics of concentrated electrolyte mixtures and the prediction of mineral solubilities to high temperatures for mixtures in the system Na−K−Mg−Cl−SO_4−OH−H_2O. Geochim. Cosmochim. Acta **51**, 2429–2443 (1987)
26. Spenser, R., Moller, N., Weare, J.: The prediction of mineral solubilities in natural waters: a chemical equilibrium model for the Na−K−Ca−Mg−Cl−SO_4−H_2O system at temperatures below 25 °C. Geochim. Cosmochim. Acta **54**, 575–590 (1990)
27. Drebushchak, V.A., Ogienko, A.G., Yunoshev, A.S.: Metastable eutectic melting in the NaCl−H_2O system. Thermochim. Acta **647**, 94–100 (2017)

28. Dubessy, J., Audeoud, D., Wilkins, R., Kosztolanyi, C.: The use of the Raman microprobe MOLE in the determination of the electrolytes dissolved in the aqueous phase of fluid inclusions. Chem. Geol. **37**, 137–150 (1982)
29. Samson, I.M., Walker, R.T.: Cryogenic Raman spectroscopic studies in the system NaCl–$CaCl_2$–H_2O and implications for low temperature phase behavior in aqueous fluid inclusions. Can. Mineral. **38**, 35–43 (2000)